30th Annual International IEEE EMBS Conference
Vancouver, British Columbia, Canada, August 20-24, 2008

Effects of I_{h} and I_{KLT} on the Response of the Auditory Nerve to Electrical Stimulation in a Stochastic Hodgkin–Huxley Model

Mohamed H. Negm[1,*], *Student Member*, and Ian C. Bruce[1,2,†], *Senior Member*
[1]School of Biomedical Engineering and [2]Department of Electrical & Computer Engineering
McMaster University, Hamilton, ON, Canada

***Abstract*— An accurate model of auditory nerve fibers (ANFs) would help in improving cochlear implant (CI) functionality. Previous studies have shown that the original Hodgkin–Huxley (1952) model (with kinetics adjusted for mammalian body temperature) may be better at describing nodes of Ranvier in ANFs than models for other mammalian axon types. However, the HH model is still unable to explain a number of phenomena observed in auditory nerve responses to CI stimulation such as long-term accommodation, adaptation and the time-course of relative refractoriness. Recent physiological investigations of spiral ganglion cells have shown the presence of a number of ion channel types not considered in the previous modeling studies, including low-threshold potassium (I_{KLT}) channels and hyperpolarization-activated cation (I_{h}) channels. In this paper we investigate inclusion of these ion channel types in a stochastic HH model. For single biphasic charge-balanced pulse, an increase in spike threshold was typically produced by inclusion of one or both of these channel types. The addition of I_{KLT} increases random threshold fluctuations in the stochastic model, particularly for longer pulse widths. Pulse-train responses were investigated for pulse rates of 200, 800, and 2000 pulse/s. Initial results suggests that both the I_{KLT} channels and I_{h} channels can produce adaptation in the spike rate. However, the adaptation due to I_{KLT} is restricted to higher stimulation rates, whereas the adaptation due to I_{h} is observed across all stimulation rates.**

I. INTRODUCTION

Several computational models have been developed to describe ANF responses to CI stimulation. Many of these have been based on the deterministic Hodgkin–Huxley (HH) model [1]. Cartee [2] showed that the temperature-adjusted HH model may be a better model for ANFs than alternative models developed for other myelinated nerve fibers. Bruce *et al.* showed that stochastic models for ANFs better predict physiological responses and psychophysical performance [3]. However, several aspects of AN responses to CI stimulation are still not accurately described by any of these models. Recent physiological studies have shown the presence of different ion channel-types in spiral ganglion cells [4], [5], [6], [7], other than the fast voltage-gated sodium ($\mathrm{Na_v}$) and delayed rectifier potassium (Kv) channels of the HH model. [4] and [7] have shown that the diversity in ion channel types and distribution affect the firing properties and participate in the signal coding and transformation in the auditory periphery.

*negmmh@mcmaster.ca
†ibruce@ieee.org

In this paper, we present a model for a patch of membrane (at the node of Ranvier of an ANF) where the low-threshold potassium (KLT) and hyperpolarization-activated cation (HPAC) channels are taken into consideration, in addition to the classical fast $\mathrm{Na_v}$ and delayed rectifier Kv of the HH model. There were several reasons for choosing these two channel types: First, Mo *et al.* [6] have observed that the I_{KLT} current is responsible for spike adaptation to a constant current injection in a patch-clamped spiral ganglion cell. Second, I_{h} is a major source of inward rectification in spiral ganglion cells [4].

Our result suggest that inclusion of I_{h} and I_{KLT} currents improve the accuracy of auditory nerve models and better explain the intrinsic response properties of ANFs to cochlear implant stimulation.

II. METHODS

A. The Model

The patch of membrane at an ANF node of Ranvier was modeled. The model comprises four voltage-gated ion channel types: 1) fast sodium $\mathrm{Na_v}$, 2) delayed-rectifier potassium Kv, 3) low-threshold potassium, and 4) hyperpolarization-activated cation channels where they control the passage of I_{Na}, I_{K}, I_{KLT}, and I_{h} currents, respectively. A passive leakage current (I_{lk}) was also included, and the leakage reversal potential (E_{lk}) was adjusted to produce a fixed resting potential of -78 mV [8]. Fig. 1 shows the equivalent electric circuit of the model. The membrane equation is:

$$C_m \frac{\mathrm{d}V_m}{\mathrm{d}t} + I_{\mathrm{Na}} + I_{\mathrm{K}} + I_{\mathrm{KLT}} + I_{\mathrm{h}} + I_{\mathrm{lk}} = I_{\mathrm{inj}}, \qquad (1)$$

where V_m is the membrane potential, C_m is the membrane capacitance, and I_{inj} is the stimulus current. Model parameter values are given in Table I.

Hodgkin and Huxley [1] assumed that the sodium channel has three independent activation particles m and one inactivation particle h, while the delayed rectifier potassium has four independent activation particles n. Using the same concept, the low-threshold potassium is considered to have four independent activation particles w and one inactivation particle z, and finally the hyperpolarization cation has one activation particle r [9]. Gating kinetics of stochastic ion channels can be modelled as continuous-time, discrete-state Markov processes [8].

978-1-4244-1815-2/08/$25.00 ©2008 IEEE.

The equations describing the Markovian transitions between states for the four channel types are:

$$\begin{array}{ccccccc} m_0h_0 & \underset{\beta_m}{\overset{3\alpha_m}{\rightleftharpoons}} & m_1h_0 & \underset{2\beta_m}{\overset{2\alpha_m}{\rightleftharpoons}} & m_2h_0 & \underset{3\beta_m}{\overset{\alpha_m}{\rightleftharpoons}} & m_3h_0 \\ \alpha_h \downarrow\uparrow \beta_h & & \alpha_h \downarrow\uparrow \beta_h & & \alpha_h \downarrow\uparrow \beta_h & & \alpha_h \downarrow\uparrow \beta_h \\ m_0h_1 & \underset{\beta_m}{\overset{3\alpha_m}{\rightleftharpoons}} & m_1h_1 & \underset{2\beta_m}{\overset{2\alpha_m}{\rightleftharpoons}} & m_2h_1 & \underset{3\beta_m}{\overset{\alpha_m}{\rightleftharpoons}} & m_3h_1 \end{array} , \quad (2)$$

$$n_0 \underset{\beta_n}{\overset{4\alpha_n}{\rightleftharpoons}} n_1 \underset{2\beta_n}{\overset{3\alpha_n}{\rightleftharpoons}} n_2 \underset{3\beta_n}{\overset{2\alpha_n}{\rightleftharpoons}} n_3 \underset{4\beta_n}{\overset{\alpha_n}{\rightleftharpoons}} n_4 \ , \quad (3)$$

$$\begin{array}{ccccccc} w_0z_0 & \underset{\beta_w}{\overset{4\alpha_w}{\rightleftharpoons}} & w_1z_0 & \underset{2\beta_w}{\overset{3\alpha_w}{\rightleftharpoons}} & w_2z_0 & \underset{3\beta_w}{\overset{2\alpha_w}{\rightleftharpoons}} & w_3z_0 & \underset{4\beta_w}{\overset{\alpha_w}{\rightleftharpoons}} & w_4z_0 \\ \alpha_z \downarrow\uparrow \beta_z & & \alpha_z \downarrow\uparrow \beta_z & & \alpha_z \downarrow\uparrow \beta_z & & \alpha_z \downarrow\uparrow \beta_z & & \alpha_z \downarrow\uparrow \beta_z \\ w_0z_1 & \underset{\beta_w}{\overset{4\alpha_w}{\rightleftharpoons}} & w_1z_1 & \underset{2\beta_w}{\overset{3\alpha_w}{\rightleftharpoons}} & w_2z_1 & \underset{3\beta_w}{\overset{2\alpha_w}{\rightleftharpoons}} & w_3z_1 & \underset{4\beta_w}{\overset{\alpha_w}{\rightleftharpoons}} & w_4z_1 \end{array} , \quad (4)$$

$$r_0 \underset{\beta_r}{\overset{\alpha_r}{\rightleftharpoons}} r_1 \ , \quad (5)$$

where α_x and β_x are the state transition rates.

Transition rate equations (α_x and β_x versus V_m) for fast Na_v and delayed rectifier Kv channels were taken directly from [8] and [10]. These sets of equations were already developed at mammalian body temperature (37 °C). However, equations for KLT and hyperpolarization-activated cation channels were developed for a temperature of 22 °C in [11]. These latter sets of equations have been adjusted from 22 °C to 37 °C following the method in [2]. We used a channel number tracking algorithm to simulate the Markov kinetics in discrete time. [8] showed that the algorithm introduced by Chow and White [12] is more efficient than other stochastic methods. The number of open channels (N_X) for each channel type X is given by

$$N_{\mathrm{Na}}(t) = N_{m_3h_1}(t)\,, \quad (6)$$

$$N_{\mathrm{K}}(t) = N_{n_4}(t)\,, \quad (7)$$

$$N_{\mathrm{KLT}}(t) = N_{w_4z_1}(t)\,, \quad (8)$$

$$N_{\mathrm{h}}(t) = N_{r_1}(t)\,, \quad (9)$$

where N_x indicates the number of channels in the state x.

B. Simulation Parameters

In order to assess the effect of adding I_{KLT} and I_{h} currents on firing properties of the membrane, we compared response properties of four versions of the model: 1) the standard model incorporating I_{Na} and I_{K} only; 2) adding I_{KLT} alone to the standard model; 3) adding I_{h} alone to the standard model; and 4) adding both I_{KLT} and I_{h}.

The stimulus current was injected intracellularly for simplicity. The current waveform was a charge-balanced symmetric biphasic pulse. The effect of flipping the leading phase polarities (hyper- and depolarizing) at pulse widths of 100, 200, 300, 500, and 700 µs per phase was evaluated.

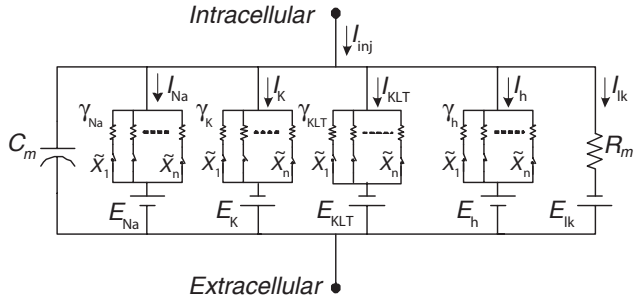

Fig. 1. Model for a patch of membrane at a node of Ranvier: C_m, R_m, γ_x, E_x are the membrane capacitance, membrane resistance, single channel conductances, and reverse potentials, respectively. $\widetilde{X_n}$ are the stochastic single-channel states (open or closed). E_{lk} is the leakage potential.

TABLE I
SUMMARY OF PARAMETERS FOR THE MEMBRANE MODEL

Parameter	Symbol	Value	Ref.
Membrane Capacitance	C_m	0.0714 pF	[13]
Membrane Resistance	R_m	1953.49 MΩ	[13]
Na Reverse Potential	E_{Na}	66 mV	[8]
K Reverse Potential	E_{K}	−88 mV	[8]
HPAC Reverse Potential	E_{h}	−43 mV	[9]
Resting Potential	V_{rest}	−78 mV	[8]
Na Channel Conductance	$\gamma_{\mathrm{Na_v}}$	25.69 pS	[8]
Kv Channel Conductance	γ_{Kv}	50.0 pS	[10]
KLT Channel Conductance	γ_{KLT}	13.0 pS	
HPAC Channel Conductance	γ_{h}	13.0 pS	
# of Na Channels	$N_{\mathrm{Na_v}}$	1000	[8]
# of K_v Channels	N_{Kv}	166	
# of K_{LT} Channels	N_{KLT}	166	
# of HPAC Channels	N_{h}	100	
KLT Channels Thermal coeff.	$\mathrm{Q10_{KLT}}$	3.0	
HPAC Channels Thermal coeff.	$\mathrm{Q10_h}$	3.3	

To test how I_{KLT} and I_{h} affect spike-rate adaptation, pulse-train stimuli of frequencies 200, 800, and 2000 pulse/s, similar to rates used in cochlear implants [14], were applied for a duration of 300 ms at three different current amplitudes (to produce first-pulse firing probabilities of 0.2, 0.5 and 0.8).

III. RESULTS

First, the influence of I_{KLT} and I_{h} on firing threshold (TH) is evaluated. Threshold is defined as the stimulus level at 50% spike probability or *firing efficiency* (FE) [15]. Fig. 2 shows firing efficiency in response to different input current levels. For each curve, data points are evaluated for one thousand simulation repetitions, and integrated-gaussian functions are fit [3]. Top and bottom panels show the cases of injecting depolarizing and hyperpolarizing phase leading biphasic pulses, respectively, at 100 µs (filled symbols) and 700 µs (open symbols) per phase. Adding I_{KLT} (♦ & ◊), I_{h} (▲ & △), or both (■ & □) shift the FE curves to the right of the standard model (● & ○) in most cases.

However, for the 100 µs-hyperpolarizing phase leading stimulus, a very slight decrease in TH from the standard model is observed for the other three channel-combinations. Curves for I_{KLT}-added are shallower than the others curves in most of the cases. Adding both I_{KLT} and I_{h} produces an additive increase in threshold.

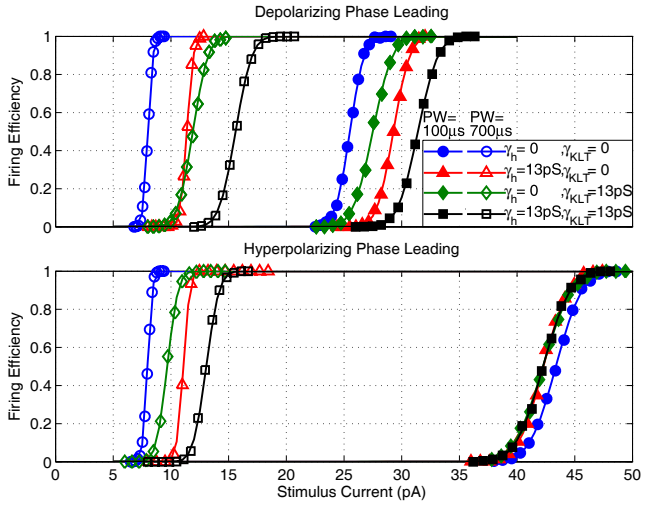

Fig. 2. Firing efficiency as a function of the stimulus current intensity for four different ion channel combinations. Response of depolarizing phase leading (top panel) and hyperpolarizing phase leading (bottom panel) for stimulus pulses at 100 µs and 700 µs pulse width per phase (filled and open symbols, respectively). Actual data from simulations (symbols) were fit with integrated-Gaussian functions (solid lines) to estimate stimulus threshold (TH) and relative spread (RS).

Inclusion of I_h and/or I_{KLT} increases thresholds for long pulse widths almost equally for depolarizing phase leading and hyperpolarizing phase leading (unfilled symbols in left panel of Fig. 3). In contrast, for short pulse widths the I_h and/or I_{KLT} channels tend to increase thresholds for biphasic pulses with a leading depolarizing phase but *decrease* thresholds for leading hyperpolarizing phase by the same amount.

The effect of I_h and I_{KLT} channels on the relationship between the relative noise level (*relative spread*, RS) and pulse width and leading polarity is given in the right panel of Fig. 3. RS is defined as the ratio of the standard deviation of the integrated gaussian to the threshold [15]. A large value of RS corresponds to a shallow FE versus current amplitude curve, indicating relatively large stochastic threshold fluctuations, whereas smaller values of RS correspond to step FE versus current curves and relatively small threshold fluctuations. I_h has only a minor effect on the RS. In contrast, adding I_{KLT} increases membrane noise significantly, especially with longer pulse widths. Including I_h in addition to I_{KLT} reduces this effect of pulse width on RS somewhat.

TH decreases exponentially with increasing pulse width, reach the asymptotic threshold at a pulse width of around 600 µs per phase–see the top panels of Fig. 4.

The effect of pulse width on RS is shown for a range of phase durations in the bottom row of Fig. 4. Here it can be seen that the pulse width has relatively little effect on RS in the model with the standard HH sodium and potassium channels ($\circ$), and I_h alone included ($*$). Inclusion of I_{KLT} alone ($\times$) or with I_h ($+$) creates an increase in RS with increasing pulse width, irrespective of leading phase. However, the RS versus pulse width effect is large for I_{KLT} alone, as noted above. These results are consistent with the physiological data of [3], in which cat ANFs stimulated by a cochlear implant were found to have an increasing RS with increasing pulse width.

Poststimulus-time histograms (PSTHs) and interspike interval (ISI) histograms for pulse-train responses are given in Figs. 5 and 6, respectively. The stimulus pulse amplitude was adjusted to give a 50% firing efficiency for the first pulse for each of the pulse rates of 200, 800, 2000 pulse/s (columns: left to right). Regardless of the group of channels included, adaptation is stronger at higher pulse rates, consistent with results from [14]. The adaptation in the standard model is due only to refractory effects. Adding I_h and/or I_{KLT} produces more adaptation than the standard model for all pulse rates. Inclusion of I_h has the largest adaptation effect (second row of Fig. 5). It was expected that I_{KLT} would be the dominant factor of adaptation as suggested in [9]. I_{KLT} still shows a degree of adaptation not observed in the standard model at higher pulse rates (third row of Fig. 5). This is supported by the ISI histogram for the model including I_{KLT} at a pulse rate of 2000 pulse/s (third row-third column of Fig. 6). Responses to stimulus pulse amplitudes producing 20% and 80% first-pulse FEs exhibit similar behavior (results not shown).

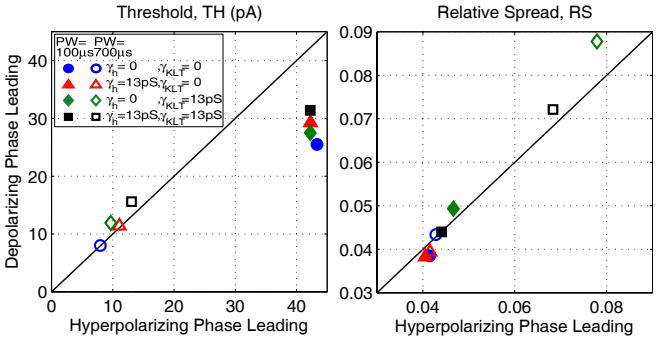

Fig. 3. Summary plots showing threshold (left panel) and relative spread (right panel) as a function of leading phase polarities for four different channel combinations. Filled and open symbols represent pulse widths at 100 µs and 700 µs per phase, respectively.

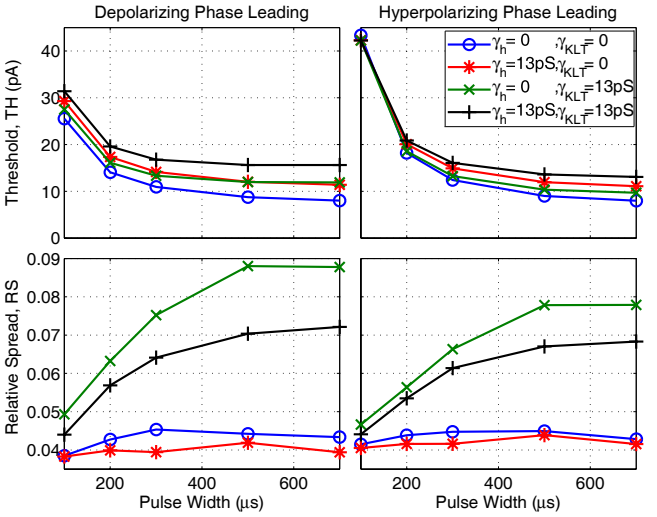

Fig. 4. TH (top row) and RS (bottom row) as a function of pulse width for both depolarizing phase leading (left column) and hyperpolarizing phase leading (right column) for four different channel combinations. Pulse widths were 100, 200, 300, 500, and 700 µs per phase

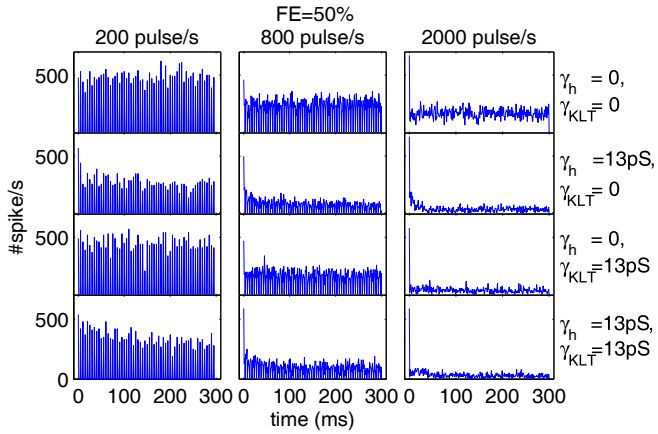

Fig. 5. PSTHs from the response to pulse-train stimuli at 50% firing efficiency. Histograms were computed for 100 simulation repetitions with time bins of 1 ms. Pulses were biphasic pulses of 100 µs/phase with depolarizing-phase leading. In each case the stimulating current amplitude was adjusted so that the first pulse in the pulse train had a 50% FE. Rows (top to bottom) represent standard, I_h added alone, I_{KLT} added alone, and I_h & I_{KLT} models, respectively. Columns (left to right) represent pulse rates of 200, 800, 2000 pulse/s.

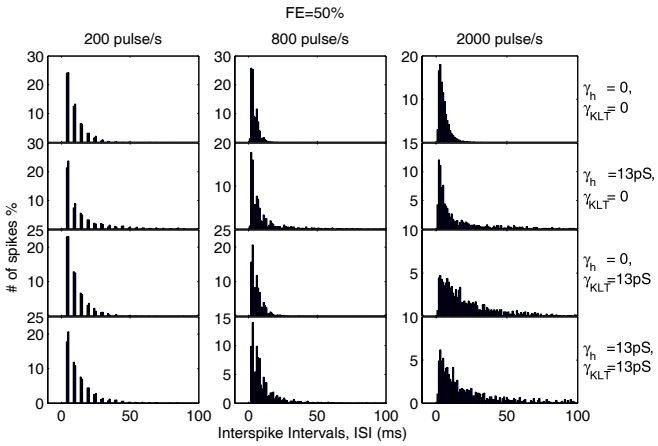

Fig. 6. ISI histograms from the response to pulse-train stimuli at 50% firing efficiency. ISI histograms were computed from the same simulations used to compute the PSTHs shown in Fig. 5. Rows (top to bottom) represent standard, I_h added alone, I_{KLT} added alone, and I_h & I_{KLT} models, respectively. Columns (left to right) represent pulse rates at 200, 800, 2000 pulse/s. Time bins are every 1 ms. Ordinate is the percentage of number of spikes to the total number of spikes.

IV. CONCLUSIONS AND FUTURE WORKS

A. Conclusions

Simulation results show that incorporating low-threshold potassium or/and hyperpolarization-activated cation channels into a stochastic HH model of ANFs has an effect on spike threshold, relative noise, and adaptation. The results help provide an interpretation of the spiking behavior of ANFs in physiological studies of CI stimulation. The I_{KLT} channel appears to explain the increase in random threshold fluctuations with increasing pulse width observed in the physiological data, while the I_h channel is a likely candidate to explain the stimulus-dependent spike-rate adaptation exhibited in responses to high-rate pulse trains. An improved understanding of the physiological response properties in CI stimulation should lead to development of new stimulation strategies for CIs that provide increased benefit for CI users.

B. Future Works

Investigating the effect of varying the inter-pulse gap is needed to get a more complete picture of the behavior of the model in response to different stimulus waveforms. A more quantitative analysis of the pulse-train responses is needed to determine how exactly the different ion channel types are contributing to the observed adaptation. Finally, a more accurate model of the I_h channel gating kinetics for spiral ganglion cells would be beneficial.

V. ACKNOWLEDGMENTS

We thank Drs. Paul Manis & Robin Davis for advice in choosing parameter values.

REFERENCES

[1] A. Hodgkin and A. Huxley, "A quantitative description of membrane current and its application to conduction and excitation in nerve," *J. Physiol.*, vol. 117, pp. 500–44, 1952.

[2] L. A. Cartee, "Evaluation of a model of the cochlear neural membrane. II: Comparison of model and physiological measures of membrane properties measured in response to intrameatal electrical stimulation," *Hear. Res.*, vol. 146, no. 1-2, pp. 153–166, Aug. 2000.

[3] I. C. Bruce, M. W. White, L. S. Irlicht, S. J. O'Leary, S. Dynes, E. Javel, and G. M. Clark, "A stochastic model of the electrically stimulated auditory nerve: Single-pulse response," *IEEE Trans. Biomed. Eng.*, vol. 46, no. 6, pp. 617–629, June 1999.

[4] Z. L. Mo and R. L. Davis, "Heterogeneous voltage dependence of inward rectifier currents in spiral ganglion neurons," *J. Neurophysiol.*, vol. 78, no. 6, pp. 3019–27, Dec. 1997.

[5] C. Chen, "Hyperpolarization-activated current (ih) in primary auditory neurons," *Hear. Res.*, vol. 110, no. 1–2, pp. 179–90, Aug. 1997.

[6] Z. L. Mo, C. L. Adamson, and R. L. Davis, "Dendrotoxin-sensitive k currents contribute to accommodation in murine spiral ganglion neurons," *The Journal of physiology*, vol. 542, no. 3, pp. 763–778, 2002.

[7] C. L. Adamson, M. A. Reid, Z. L. Mo, J. Bowne-English, and R. L. Davis, "Firing features and potassium channel content of murine spiral ganglion neurons vary with cochlear location," *The Journal of comparative neurology*, vol. 447, no. 4, pp. 331–350, Jun 10 2002.

[8] H. Mino, J. T. Rubinstein, and J. A. White, "Comparison of algorithms for the simulation of action potentials with stochastic sodium channels," *Ann. Biomed. Eng.*, vol. 30, no. 4, pp. 578–587, Apr. 2002.

[9] J. Rothman and P. Manis, "The Roles Potassium Currents Play in Regulating the Electrical Activity of Ventral Cochlear Nucleus Neurons," *Journal of Neurophysiology*, vol. 89, no. 6, pp. 3097–3113, 2003.

[10] H. Mino, J. T. Rubinstein, C. A. Miller, and P. J. Abbas, "Effects of electrode-to-fiber distance on temporal neural response with electrical stimulation," *IEEE Trans. Biomed. Eng.*, vol. 51, no. 1, pp. 13–20, Jan. 2004.

[11] J. S. Rothman and P. B. Manis, "Kinetic analyses of three distinct potassium conductances in ventral cochlear nucleus neurons," *Journal of neurophysiology*, vol. 89, no. 6, pp. 3083–3096, Jun 2003.

[12] C. C. Chow and J. A. White, "Spontaneous action potentials due to channel fluctuations," *Biophys. J.*, vol. 71, pp. 3013–3021, December 1996.

[13] I. Bruce, "Implementation Issues in Approximate Methods for Stochastic Hodgkin–Huxley Models," *Annals of Biomedical Engineering*, vol. 35, no. 2, pp. 315–318, 2007.

[14] F. Zhang, C. Miller, B. Robinson, P. Abbas, and N. Hu, "Changes Across Time in Spike Rate and Spike Amplitude of Auditory Nerve Fibers Stimulated by Electric Pulse Trains," *JARO-Journal of the Association for Research in Otolaryngology*, vol. 8, no. 3, pp. 356–372, 2007.

[15] C. Miller, P. Abbas, B. Robinson, J. Rubinstein, and A. Matsuoka, "Electrically evoked single-fiber action potentials from cat: responses to monopolar, monophasic stimulation," *Hearing Research*, vol. 130, no. 1-2, pp. 197–218, 1999.